



Article

Analysis of Fire-Induced Circulations during the FireFlux2 Experiment

Jeremy T. Benik ¹, Angel Farguell ¹, Jeffrey D. Mirocha ², Craig B. Clements ¹ and Adam K. Kochanski ^{1,*}

- Wildfire Interdisciplinary Research Center, Department of Meteorology & Climate Science, San José State University, San Jose, CA 95192-0126, USA; jeremy.benik@sjsu.edu (J.T.B.)
- ² Lawrence Livermore National Laboratory, Livermore, CA 94550-9234, USA
- * Correspondence: adam.kochanski@sjsu.edu

Abstract: Despite recent advances in both coupled fire modeling and measurement techniques to sample the fire environment, the fire-atmosphere coupling mechanisms that lead to fast propagating wildfires remain poorly understood. This knowledge gap adversely affects fire management when wildland fires propagate unexpectedly rapidly and shift direction due to the fire impacts on local wind conditions. In this work, we utilized observational data from the FireFlux2 prescribed burn and numerical simulations performed with a coupled fire-atmosphere model WRF-SFIRE to assess the small-scale impacts of fire on local micrometeorology under moderate wind conditions (10-12 m/s). The FireFlux2 prescribed burn provided a comprehensive observational dataset with in situ meteorological observations as well as IR measurements of fire progression. To directly quantify the effects of fire-atmosphere interactions, two WRF-SFIRE simulations were executed. One simulation was run in a two-way coupled mode in which the heat and moisture fluxes emitted from the fire were injected into the atmosphere, and the other simulation was performed in a one-way coupled mode for which the atmosphere was not affected by the fire. The difference between these two simulations was used to analyze and quantify the fire impacts on the atmospheric circulation at different sections of the fire front. The fire-released heat fluxes resulted in vertical velocities as high as 10.8 m/s at the highest measurement level (20 m above ground level) gradually diminishing with height and dropping to 7.9 m/s at 5.77 m. The fire-induced horizontal winds indicated the strongest fire-induced flow at the lowest measurement levels (as high as 3.3 m/s) gradually decreasing to less than 1 m/s at 20 m above ground level. The analysis of the simulated flow indicates significant differences between the fire-induced circulation at the fire head and on the flanks. The fire-induced circulation was much stronger near the fire head than at the flanks, where the fire did not produce particularly strong cross-fire flow and did not significantly change the lateral fire progression. However, at the head of the fire the fire-induced winds blowing across the front were the strongest and significantly accelerated fire progression. The two-way coupled simulation including the fire-induced winds produced 36.2% faster fire propagation than the one-way coupled run, and more realistically represented the fire progression.

Keywords: fire-induced circulations; WRF-SFIRE; FireFlux2; experimental fires; fire modeling; fire wind



Citation: Benik, J.T.; Farguell, A.; Mirocha, J.D.; Clements, C.B.; Kochanski, A.K. Analysis of Fire-Induced Circulations during the FireFlux2 Experiment. *Fire* **2023**, *6*, 332. https://doi.org/10.3390/ fire6090332

Academic Editor: Alistair M. S. Smith

Received: 11 July 2023 Revised: 11 August 2023 Accepted: 21 August 2023 Published: 24 August 2023



Copyright: © 2023 by the authors. Licensee MDPI, Basel, Switzerland. This article is an open access article distributed under the terms and conditions of the Creative Commons Attribution (CC BY) license (https://creativecommons.org/licenses/by/4.0/).

1. Introduction

Fire behavior may be significantly impacted by fire-induced perturbations to the atmosphere. As the fire releases heat and moisture from fuel combustion, the fire induces turbulent circulations by altering the local thermal structure of the lower atmospheric boundary layer [1]. These fire-induced perturbations in turn impact local fire Rate of Spread (ROS). To assess how the fire induces its own circulations (fire winds), observations and simulations of fires are necessary to determine how the fire changes local conditions. There have been multiple experiments conducted to observe fire–atmosphere coupling processes by sampling the fire environment. Some experiments intended to collect data on

the fire-induced circulations, and other experiments were more focused on other aspects such as smoke transport and how fires impact the structure of the atmosphere [1–5]. Such experiments are crucial to better our understanding of how fire circulations impact the local conditions and fire spread. In this study, we used a prescribed fire with multiple instruments within the burn plot to sample how the weather conditions change in response to the Fire Front Passage (FFP). The insight into the fundamental fire–atmosphere coupling processes that impact wildfire behavior is critical to improve our understanding of fire behavior in response to fire-induced winds [6,7]. Although experimental data can provide invaluable information for the analysis of fire-induced circulations, observations alone cannot be used to systematically quantify the fire winds. On one hand, the observed winds are a result of both the ambient wind fluctuations as well as fire winds. On another hand, the limited sampling resolution (typically just a few locations within the burn plot) makes reconstructing the 3D flow near the fire and quantifying fire-induced perturbations based on observation alone, not feasible. However, with the help of coupled fire-atmosphere simulations, it is possible to overcome these limitations. Numerical experiments with and without fire-atmosphere feedback initialized to render experimental burns (both in the sense of the meteorological conditions as well as the fuel and terrain) allow us to analyze and quantify the fire impacts by subtracting variables from one-way coupled simulation from the two-way coupled ones.

The experimental burn used in this study is the FireFlux2 (FF2) experimental burn. This burn took place in Texas in 2013 in a flat prairie with nearly homogenous grassy fuels. It was conducted to better understand micrometeorological aspects of fire spread [5], and occurred during red flag warning conditions (high winds and low relative humidity), which allowed the fire to spread much faster than in typical experimental fires. Four meteorological towers were installed within the burn plot, each equipped with anemometers and thermocouples at varying heights, as well as pressure sensors, ground thermocouples, and a SODAR that collected data on how the fire affects local atmospheric conditions. Additionally, two infrared (IR) cameras collected video footage showing the fire progression. There was also a radiosonde launched near the time of ignition to gather information about the vertical structure of the atmosphere before the burn.

The FF2 experiment was a follow-up from the original FireFlux experiment that occurred in 2006. The FireFlux burn provided a unique opportunity for rigorous validations of many coupled fire–atmosphere models [8–11]. The unique characteristic of the FF2 burn compared with FireFlux stems from the fact that the FF2 burn was conducted under stronger winds, with more instruments, and with improved IR fire mapping as well as more comprehensive meteorological measurements. The purpose of the FireFlux burn was to study fire–atmosphere interactions during a fast-spreading grass fire by measuring the wind, turbulence, and temperature [9]. The authors found the FireFlux burn altered the local conditions by generating strong turbulence (4–5×greater than ambient conditions [4]) which could be seen downstream from the fire front due to the downward transport of higher momentum [4]. This indicated that the fire not only impacts conditions at the fire front, but well ahead of the fire front as well.

Combining these observations from the FireFlux burn with model simulations allows for a new perspective into how fire-induced perturbations impact the fires' propagation and surrounding conditions. One experiment that conducted an analysis using the FireFlux burn occurs in [11] where they use the ForeFire/Meso-NH model in a Large Eddy Simulation (LES) configuration to determine how fire-induced perturbations impact the shape of the fire, the fire forcing on the atmospheric flow in the lowest layers, and the impacts of the fire-induced wind on the surrounding atmosphere [11]. They found that the shape of the fire front is strongly affected by the fire-induced winds as the fire head becomes narrower and propagates faster, which matches the observations [4,11]. With a similar fire shape, the heat flux injected in the atmosphere as well as the wind perturbations in both the model and observations were consistent. The only difference between the model and observations was a slight wind shift which occurred during the burn and impacted the

fire progression. As the fire propagated through the towers, it produced downdrafts just before FFP, which occurred in both the simulations and observations, then a fast increase in winds when the fire front was under the tower due to heating [11]. After that, downdrafts occurred after FFP in both the simulation and observations [11]. This behavior indicates how the fire-induced updrafts and downdrafts impacted the surrounding atmosphere, creating vertical perturbations.

Similar experiments were analyzed based on Australian grassfires from [12] and numerical simulations from [13] using the University of Utah's Large-scale Eddy Simulation model [14]. These experiments were performed to examine the variability in fire behavior under two types of atmospheric boundary layers using a coupled fire atmosphere model. However, Ref [14] also analyzed how the fire-induced winds impact the ROS using a one-way coupled simulation and a two-way coupled simulation. They found that the two-way coupled simulation tended to spread more in the downwind direction compared to the one-way coupled simulation, which spread more along the flanks of the fire. This indicated that the fire-induced winds affected the overall shape of the fire.

Another set of numerical experiments using a coupled fire–atmosphere model was conducted in [15] to test how fires impact the surrounding conditions and how they create their own weather. Three different experiments were conducted under different ambient conditions with three short fire lines, and two longer fire lines with homogeneous fuels. The different ambient conditions consisted of varying wind intensities. In the simulations with the weak wind, the position of the fire front remained mostly stationary and the fireline began to break up [15]. With stronger winds, the fire front progressed much faster and took on a conical shape [15]. These shapes were explained by how the lower-level convergence produced by the hot convective columns tilted downstream from the fire front [15]. This tilt shifted the center of the convergence ahead of the fire front, so that with faster ambient winds, the tilt was stronger, and the center of the convergence zone was farther downwind from the fire front [15]. Because of the locations ahead of the fire front, the convergence increased the flow across the fire front, and accelerated fire progression. Under weak ambient conditions, the fire line began to break up without generating as strong of a convective column due to limited propagation speed and intensity.

Despite the extensive previous knowledge on how fire-induced circulations impact fire spread and how they alter the local conditions both at the fire front and ahead of it, there still exists a knowledge gap on the circulations at both the head and flanks of the fire front, as well as how strong fire winds are. By using a model simulation that has been verified with field observations taken during the FF2 experiment, we can accurately quantify the effects from a fire on the local conditions and compare the head and flank circulations. With this study, we can then investigate fire–atmosphere interactions and their impacts on local weather conditions and the fire spread.

2. Methods

To analyze fire-induced circulations at the head and flanks of the fire, we used two idealized WRF-SFIRE simulations of the FF2 experimental burn—a two-way coupled run in which fire-released heat and moisture fluxes were fed to the atmosphere to resolve the fire-induced winds, and the one-way coupled simulation in which fire-released heat and moisture fluxes were neglected. These runs allowed us to investigate the impact of fire-atmosphere interactions on local winds and the fire propagation, and the difference between the wind fields and the rate of spread from these simulations allowed us to quantify the fire winds and the effects of fire-atmosphere coupling on fire propagation.

WRF-SFIRE [2,16–18] used in this study is a two-way coupled fire–atmosphere model that couples the Weather Research Forecasting (WRF) model with a fire spread model (SFIRE). SFIRE is a fire spread model that incorporates the level set method [16] using the semi-empirical Rothermel fire spread model [19]. WRF-SFIRE uses two separate meshes: a three-dimensional atmospheric mesh and a refined fire mesh at the surface [9]. The model can simulate both idealized and real cases and is fast enough to be used for operations.

WRF-SFIRE has been used to simulate both wildfires near real time (e.g., [20,21]) as well as experimental fires (e.g., [5,9]). WRF-SFIRE numerical simulations of experimental burns were also conducted to support planning of experimental burns (e.g., [5]). Models like WRF-SFIRE have been developed to represent the first-order effect of fire–atmosphere interactions at landscape-to-micrometeorological scales [6]. Coupled fire–atmosphere simulations along with observational data can therefore be used to investigate small-scale fire–atmosphere processes impacting near-fire circulations that control fire behavior.

The set-up for the FF2 WRF-SFIRE simulation consisted of one domain with an atmospheric grid of 200 × 320 grid points (west-east × south-north) and a time step of 0.0025 s. Each grid point in the atmospheric mesh was 5 m \times 5 m with 80 vertical levels reaching 1200 m. The fire grid contained 2000×3200 grid points with each point being $0.5 \text{ m} \times 0.5 \text{ m}$ in size. The model used a stretched vertical mesh with the first model level placed at 1.05 m above the ground and the vertical resolution gradually decreased to an average of 27.75 m at the top of the domain. At the top of the domain the simulation used a sponge layer. This simulation was run on flat ground and used fuel category 3 in the Albini categories (tall grass) with a 14% fuel moisture, and fuel load set to 0.64 kg/m² according to the FF2 fuel observations taken prior to the burn. Tall grass was chosen as it best represents the fuel at the burn site. Table 1 contains more details about the FF2 simulation set-up. To initialize winds in the model, we used data from the sounding launched at 14:24 CST (as seen in Figure 1) along with the SODAR and tower data to create a vertical wind profile representative of the initial conditions before the burn. We then averaged the wind speed from all the towers at all available heights before ignition (from 15:00-15:04) to initialize the model. Each tower shown in Figure 2 was equipped with sonic anemometers at different heights that recorded both temperature and wind, as well as thermocouples that recorded temperature. These anemometers are capable of measuring temperatures over 350 °C as they were specifically designed and calibrated for fire applications. Data from these anemometers were used to initialize the model and validate the simulated winds. The peak temperature from sonic anemometers was used to verify the timing of the FFP at the tower locations. The thermocouples provided information on the duration as well as the vertical structure of the thermal perturbation, which was used to verify the simulated temperature profile at each tower. A full list of the instruments can be found in [5].

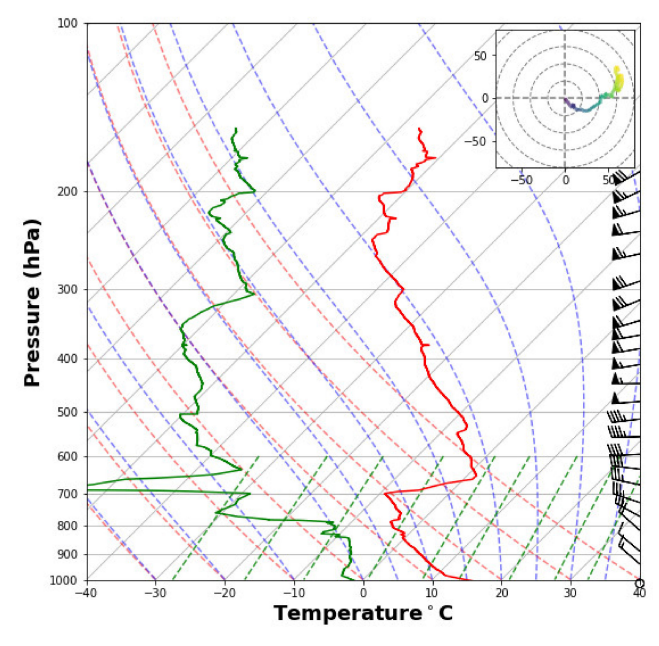


Figure 1. Skew-T plot of the sounding launched at 14:24 CST at the FF2 burn site. The red line represents the temperature in Celsius and the green line represents the dew point temperature in Celsius. The dashed blue lines represent the moist adiabat, the red dashed lines are the dry adiabat, and the green dashed lines represent the water vapor mixing ratio.

Fire **2023**, *6*, 332 5 of 19

Table 1. WRF-SFIRE FF2 simulation set-up.

Simulation Type	LES
Horizontal domain size	1000 m × 1600 m
Atmospheric Mesh	$200\times320\times80$
Horizontal resolution (atmospheric mesh)	5 m
Model top	1200 m
Vertical resolution	1.05 m at the surface to 27.75 m at the model top
Fire mesh	2000 × 3200
Horizontal resolution (fire mesh)	0.5 m
Simulation length	40 min
Time step	0.0025 s
Subgrid scale closure	1.5 TKE (Turbulence Kinetic Energy)
Lateral boundary conditions	Open
Surface layer physics	Monin–Obukhov similarity theory (sf_sfclay_phys = 1)
Land surface model	SLAB 5-layer MM5 model (sfsurface_physics = 1)
Thickness of the ignition line	1 m
Heat extinction depth	6 m
Fuel depth	1.25 m
Ground fuel moisture	14%
Fuel load	$0.64 \mathrm{kg/m^2}$
Fuel type of the burnt area	3 (Tall grass)
Inflow wind profile	Tower data + SODAR + Radiosonde
Inflow wind direction	310
WRF-SFIRE Version	4.4 (commit 3c960d725cfab7597bcfcdecb5bc55f70a7e640e)

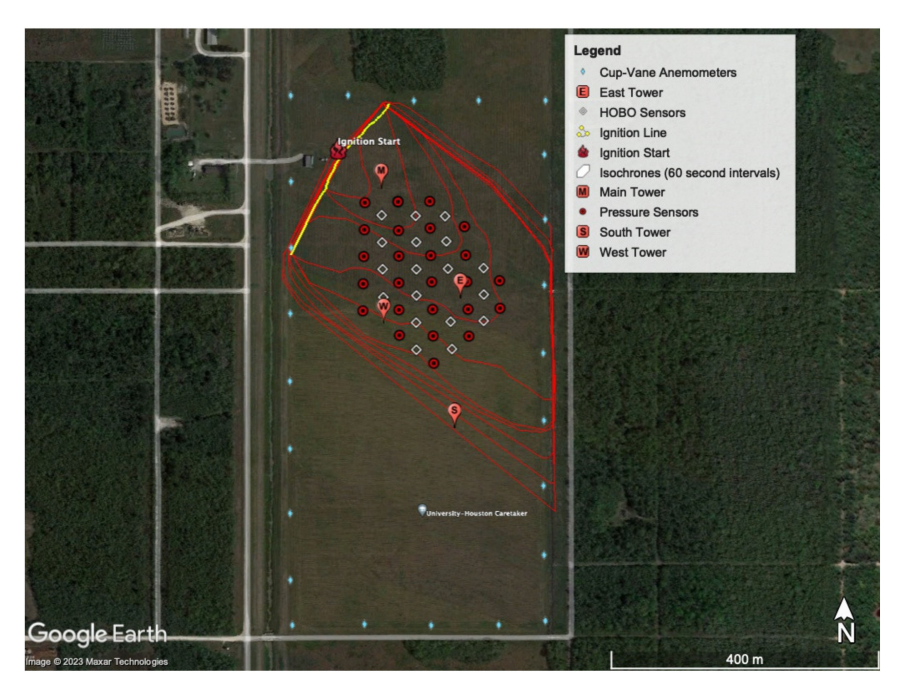


Figure 2. Map of the FF2 experimental plot showing instrumentation locations and fire perimeters.

The simulation started at 14:50 CST and the initial 14 min were used to spin up the atmospheric model before the fire ignition. The fire was ignited using two walking ignitions starting at 15:04:08 CST, representing the GPS-ed firefighters' paths. The simulation was run for 40 min (14:50–15:30 CST) which was sufficient to simulate the FFP through the locations of all meteorological towers. To quantify fire-induced circulations after completing the coupled simulation, another identical simulation but with the fire-induced fluxes turned off was executed. The results from this run, referred to as a one-way coupled simulation, were subtracted from the fully coupled simulation to quantify fire-induced winds and thermal perturbations.

The towers located within the burn plot provided observations of the fire ROS as well as the circulations at both the flanks and the head of fire. The East Tower (ET) and Main Tower (MT) sampled the head fire, while the West Tower (WT) and South tower (ST) sampled the flank of the fire. Therefore, the towers provided not only an indication of the ROS, but also sampled the fire-induced circulations at the head and at the flanks of the fire. The observational data along with the numerical experiments were used to investigate and contrast fire effects at the head and at the flanks.

3. Results and Discussion

3.1. Rate of Spread

To find the ROS of the fire, we utilized the anemometers on all four towers. Figure 3 shows the temperature from the observations and simulation from 5.28 to 5.77 m Above Ground Level (AGL) at the locations of the main tower and short towers. The time at which the temperature reached a maximum corresponds to the FFP at the towers and can be used to investigate the fire-front arrival time as well as the overall fire spread at the head and flanks of the fire. The timing of the fire-front passage can be estimated by analyzing the spikes in temperature associated with the times when the fire reached the towers. The simulation captured well the timing of the passage of the head fire through the MT (Figure 3a) and the ET (Figure 3b). The onset of the temperature increase associated with the FFP was nearly perfectly captured by the model at the MT and within about 20 s at the ET. However, more significant differences in the timing of the FFP between the simulation and observations occurred at the flanks of the fire. The temperature data suggest that the model overpredicted the ROS at the WT (Figure 3c) and underpredicted the ROS at the ST (Figure 3d). To estimate the ROS at each tower, we assessed the distance from the ignition point to the towers and divided that by the time where the temperature reached the maximum (in both the simulation and observations). The estimated ROS values at the tower locations can be seen in Table 2. The observed values presented there show the fire spread quickly at the head fire (MT and ET) with the ROS over 1 m/s, then the fire spread slowed down at the flanks of the fire (at the WT). A wind shift later in the burn then caused the fire to spread more towards the ST, which increased the ROS for that location. The two-way coupled simulated values in Table 2 show that the ROS was much faster at the head fire compared to the flanks. The simulated head fire spread at 1–1.45 m/s compared to the flanks which spread much slower at less than 1 m/s. The comparison between the ROS in the two-way and one-way coupled simulations indicates that neglecting the fireinduced winds leads to an underestimated fire progression. Consequently, when compared to observations the two-way coupled simulation resolving the fire winds rendered the fire behavior much more realistically than the on-way coupled one. The bias in the ROS averaged over all tower locations in the simulation neglecting the fire winds was 43.1%, while the two-way coupled simulation was just 6.3%.

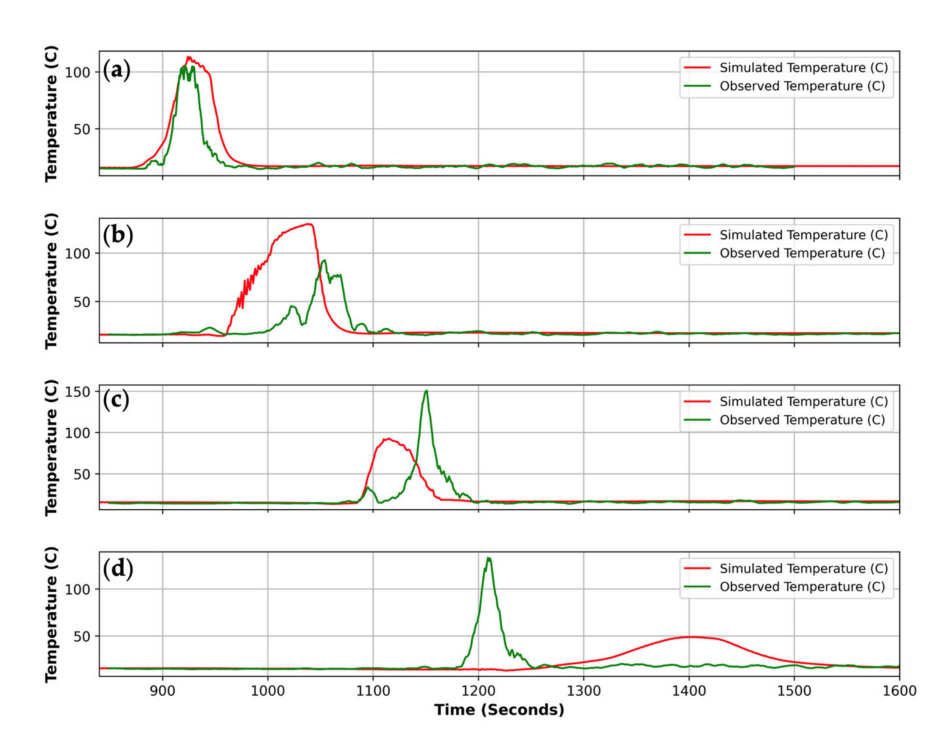


Figure 3. Time series of the simulated temperature compared to a 10 s rolling average of the observations from the 4 towers: (a) MT, (b) ET, (c) WT, and (d) ST.

Table 2. Comparison of the ROS at all towers.

Tower	MT	ET	WT	ST	Average
Observed ROS (m/s)	1.04	1.33	0.84	1.2	1.1
Two-Way Coupled Simulated ROS (m/s)	1	1.45	0.95	0.78	1.05
One-Way Coupled Simulated ROS (m/s)	0.69	0.89	0.64	0.61	0.71
% Difference Between Two-Way Coupled and Observations	-3.92	8.63	12.29	-42.42	-6.36
% Difference Between One-Way Coupled and Observations	-40.46	-39.64	-27.03	-65.19	-43.08

The discrepancies between the simulated and observed timing of the FFP at the flank were due to the change in fire propagation later into the experiment associated with this shift. This can be seen in Figure 4, where the simulated fire perimeters are compared to the IR fire perimeters. During the burn, a slight wind shift occurred which changed the main axis of the fire propagation. This could not be captured in the idealized simulation where the winds are initialized only at the beginning of the simulation and then used for the entirety of the simulation along with the open boundary conditions. The wind shift made the fire propagate more in the southern direction than indicated by the simulation. This did not affect the head fire as much since the fire had already propagated through the MT and ET before this wind shift occurred. With the ROS validated at the head of the fire, we then analyzed how well the simulation captured the thermal plume structure of the fire compared to observations.

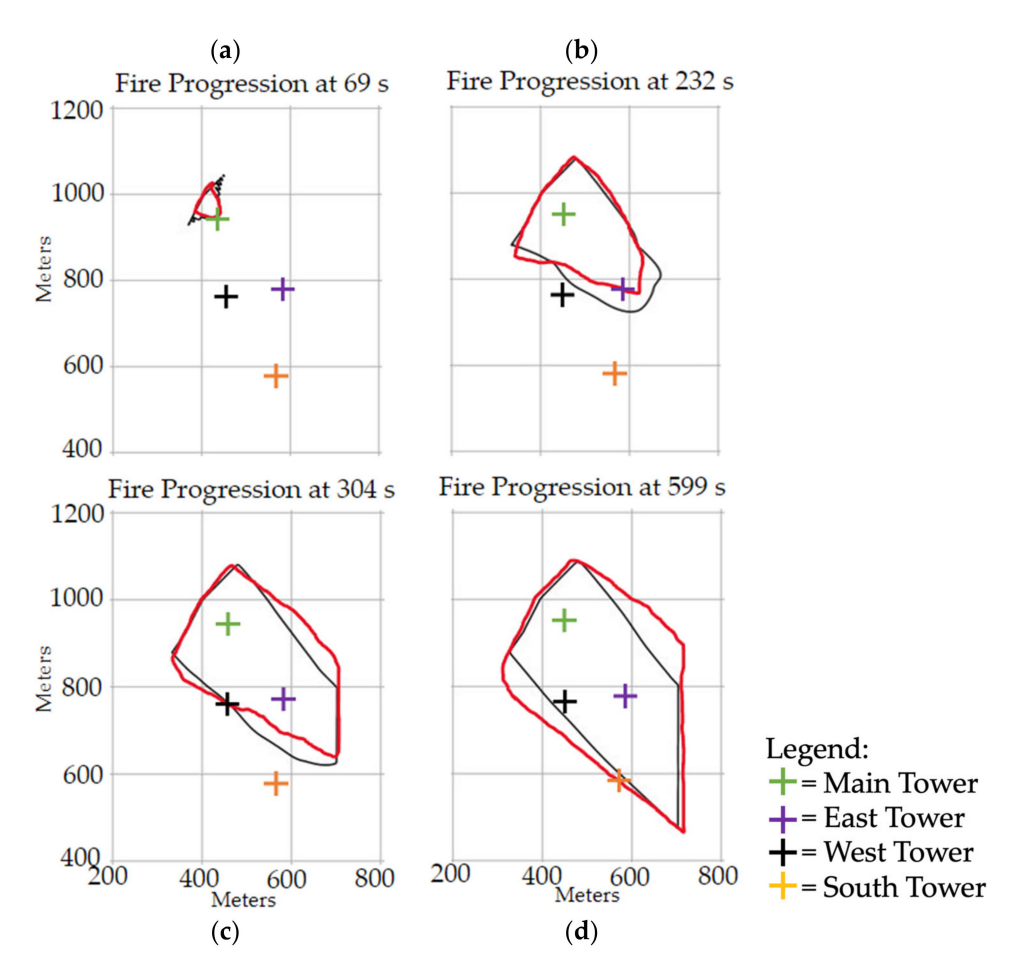


Figure 4. Simulated fire perimeter (black) compared to observed fire perimeter using IR sensors (red) at times when the observed IR perimeter intersected the towers. Simulated and observed time at the MT (**a**) is 69 s after ignition, at the ET (**b**) is 232 s after ignition, at the WT (**c**) is 304 s after ignition, at the ST (**d**) is 599 s after ignition.

3.2. Analysis of the Thermal Plume Structure

The temperature time series between 5.28 m and 5.77 m discussed in the previous section gives a good indication of the FFP timing but is not sufficient to verify the vertical extent of the thermal disturbance. Therefore, to analyze the thermal plume structure, we used the thermocouples installed on each tower. The MT had thermocouples mounted at heights from 0.3 m to 45 m (AGL), while the short towers had thermocouples installed between 0 m and 9 m AGL.

Both the duration and the vertical extent of the plume agree with the observations, which indicates that the simulation realistically represented the thermal plume structure at the head of the fire. The fire-induced temperature perturbation at the MT (Figure 5a,b) extended up to 20 m both in observations, and simulations. The model also realistically captured the duration of the thermal perturbation lasting about 50 s in both the simulation and observations. This agreement indicates the width of the convective plume column passing the tower was well represented. Looking at the ET (Figure 5c,d), the model resolved the temperatures above 180 °C at about 5 m, which is consistent with what was observed during the burn. However, duration of the thermal perturbation was overestimated. Most probably this was due to some discrepancies between the simulated and observed shape of the fire-front head when it crossed the ET. As shown in Figure 4b, the simulated fire front was broader than the observed one, and its tip was shifted to the south from the tower compared to the observations, which could result in the observed discrepancies in the temperature field. Still, the overall agreement between the observed and simulated thermal

structure at the head fire builds confidence in the simulation and motivates the investigation of the circulations induced by the fire-induced buoyancy and pyro-convection.

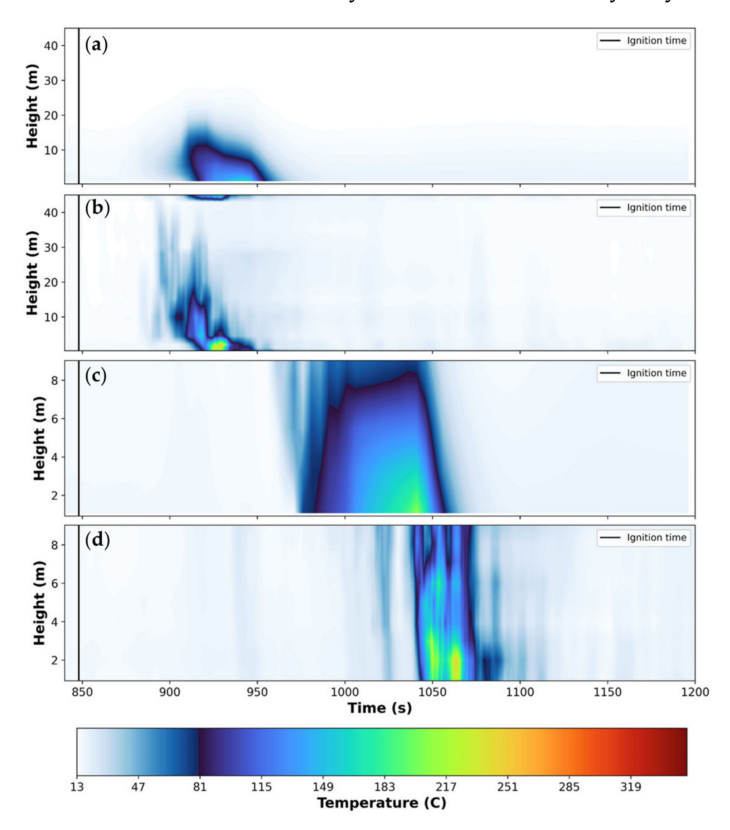


Figure 5. Time series of the temperature from the simulation and 10 s rolling average of the temperature from the observations at the MT and ET. Simulated temperatures at the MT (a) and ET (c) and observed temperature from the thermocouples at the MT (b) and ET (d).

3.3. Vertical Wind Analysis

The thermal perturbations induced by the fire can generate buoyant updrafts changing the vertical and horizontal circulation near the fire front. Therefore, after the analysis of the vertical temperature structure during the fire-front passage, the vertical winds were assessed. It was done to determine if the model properly accounted for the heat injected into the local atmosphere, which would then cause buoyant forces and consequently updrafts. The MT was used in this section because it had three anemometers reaching 20 m, which allowed for a more comprehensive analysis on the impacts from the heat output at higher levels than the short towers which only had one anemometer near the surface.

The observations in Figure 6 display the strongest vertical winds occurring at 20 m, then 10 m, and finally the weakest updrafts occurring at 5.77 m AGL. The simulated values (Figure 6) have the strongest updrafts occurring at 10 m, then 5.77 m, and finally the weakest updrafts occur at 20 m. We hypothesize that, in the simulation, the fire-induced circulation was not fully developed at the time it had propagated through the MT. It has to be noted that the fire front was already passing the MT while the ignition was still progressing, and the fire reached the MT very fast, roughly about one minute since the ignition start (see Figure 4a). The thermal plume in the observations presented in Figure 5b is significantly hotter (250 °C) compared to the simulated temperatures in Figure 5a reaching only 163 °C. We hypothesize that the underestimated buoyancy led to weaker convection produced in the simulation which manifested in undeveloped updrafts at higher elevations (i.e., 20 m AGL). Consequently, the vertical winds peaked at 10 m and did not extend vertically as high as in the observations. However, both the simulation and observations follow a similar trend with downdrafts occurring before FFP, then a sharp increase in the winds when the fire was underneath the tower due to the heating, then downdrafts after FFP, which is

consistent with [11] who observed similar trends in their experiment with FireFlux. With this validation between the simulation and observations, we then analyzed the fire-induced winds at the head and flanks of the fire.

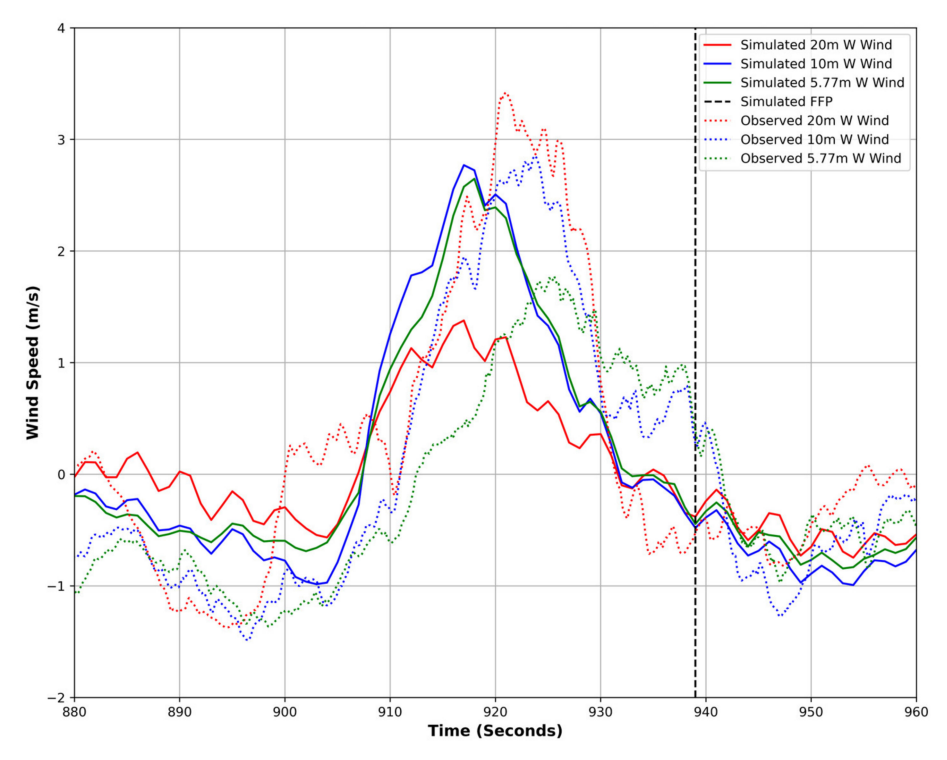


Figure 6. Simulated vertical velocities compared to the observed vertical velocities with a 10 s rolling average at 20 m, 10 m, and 5.77 m at the MT.

3.4. Analysis of Fire-Induced Circulations

After the basic validation of the thermal plume structure, we then focused on the horizontal wind associated with the fire-front passage. This is critical due to the direct impact of the horizontal fire winds on the rate of the fire spread. Later in the text we compare simulations at the head and the flanks to better understand the impact of fire-induced circulation on fire dynamics. By analyzing the magnitude of the fire winds we try to assess to what degree the fire-induced horizontal circulation could have impacted the fire behavior.

3.4.1. Circulation at the Fire Head

We start from the analysis of fire winds at the MT, computed as a difference between the two-way coupled and one-way coupled simulation. As can be seen in Figure 7, the fire-induced horizontal circulation was the strongest at the surface and gradually decreased with height. The strongest fire-induced winds occurred at 5.77 m AGL with winds greater than 3 m/s, then decreased to 1.5 m/s at 10 m, and finally decreased even more to less than 0.5 m/s at 20 m. These winds indicate that the fire-induced winds originated near the surface and were diminishing at higher elevations. The peak in the fire-induced winds occurred before the FFP and extended for about 100 s, indicating that the winds created by the fire affected the local conditions driving the fire-front propagation. Similar conditions were experienced in [4] with turbulence induced from the fire seen downstream from the fire front, which impacted the winds ahead of the fire front. After the FFP, the winds decreased rapidly but remained slightly elevated for a prolonged time as the fire continued to burn.

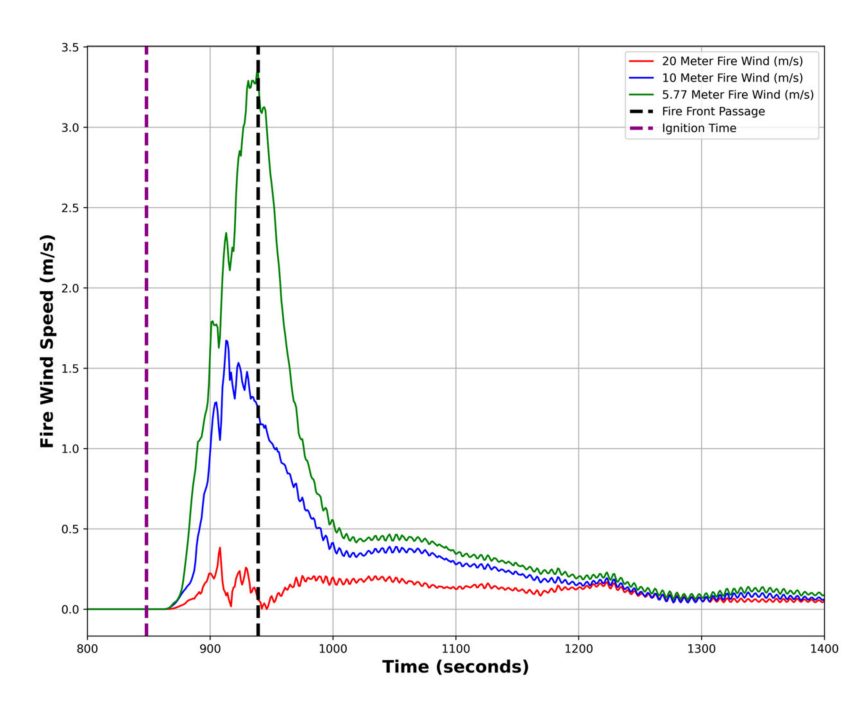


Figure 7. Time series of simulated fire winds at 20 m (red), 10 m (blue), and 5.77 m (green) AGL at the MT.

To determine the impact from the fire-induced winds on ambient conditions, we created a cross-section (as seen in Figure 8a) of the ambient winds, fire-induced vertical velocities, and the fire ground heat flux (as seen in Figure 8b). The head fire produced not only stronger winds at the surface, as seen in Figure 8b, but also an updraft zone between two downdraft zones indicated by negative values in Figure 6. Figure 8b shows that the convective column is pushed ahead of the fire front so that the inflow into the base of the column induces the cross-fire wind that accelerates its progression. Since this inflow occurs near the ground, the acceleration in the surface winds is the most intense at the lowest elevations behind and at the fire front and decreases with height, as previously seen in time series presented in Figure 7. Although the most intense horizontal winds were present near the ground, the strongest updrafts occurred ahead of the fire front between 40 and 60 m AGL. The shape of the updraft zone presented in Figure 8b indicates a narrow conic shape near the ground and extending with height, producing more inflow near the ground.

The inflow into the convective column located ahead of the fire front significantly accelerates horizontal winds controlling the fire ROS. The orange wind streamlines shown in Figure 8b occur exactly over the peak heat flux represented as the blue line on the panel below. This alignment confirms that the accelerated winds are located over the fire front, establishing the dynamical interaction between the fire-induced winds and the fire behavior, which, as shown later, results in increased ROS.

The vertical structure of the fire-induced winds with the strongest winds located near the ground and decreasing with height suggests a presence of a low-level fire-induced jet that could lead to a potential local reversal of the typical logarithmic wind profile. To investigate whether that is the case, in Figure 9, we analyzed the vertical profile at the MT location before the ignition at 15:04:08 (blue lines) and during the FFP (red lines). Figure 9 shows the wind speed vertical profile as simulated by the model (solid lines) and observations at the MT (dashed lines). Both the simulation and observation indicate wind profile reversal associated with the FFP. This wind profile reversal results from the horizontal flow into the convective column super positioned over the ambient winds. The fire, by heating the air column, causes air masses to rise and create a pyro-convective column. This convective column is advected downwind of the fire front (as seen in Figure 8b), causing the strongest fire-induced vertical wind to occur ahead of the fire front). The low pressure created as the air mass was driven up induces surface convergence ahead of the fire front as

seen in Figure 10, which is consistent with [15], who noted that under fast ambient winds, the center of the convergence zone was pushed downwind of the fire front.

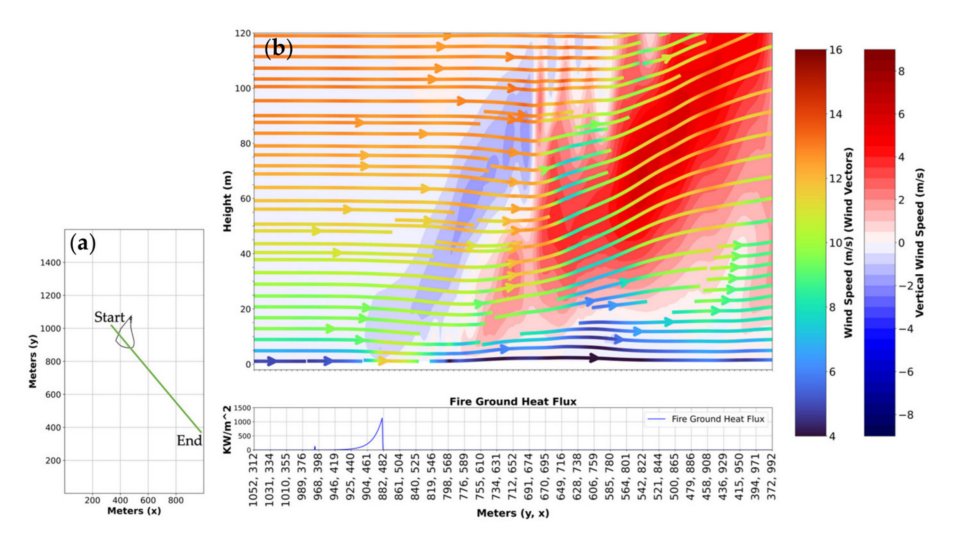


Figure 8. (a) Fire-front position (black polygon), and the orientation of the cross-section (green line). (b) Vertical cross-section showing winds from the two-way coupled simulation taken at 15:06:06 CST and the fire ground heat flux showing the position and intensity of the fire. The streamlines are color coded according to the wind speed magnitude; the shading shows the magnitude of the fire-induced vertical velocity.

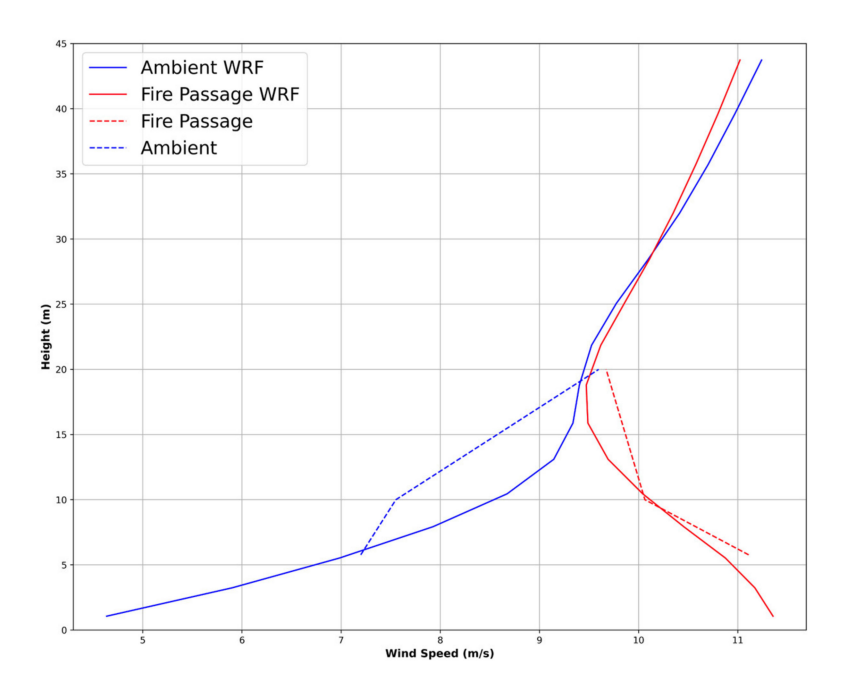


Figure 9. Vertical profile of the ambient conditions and FFP conditions at the main tower.

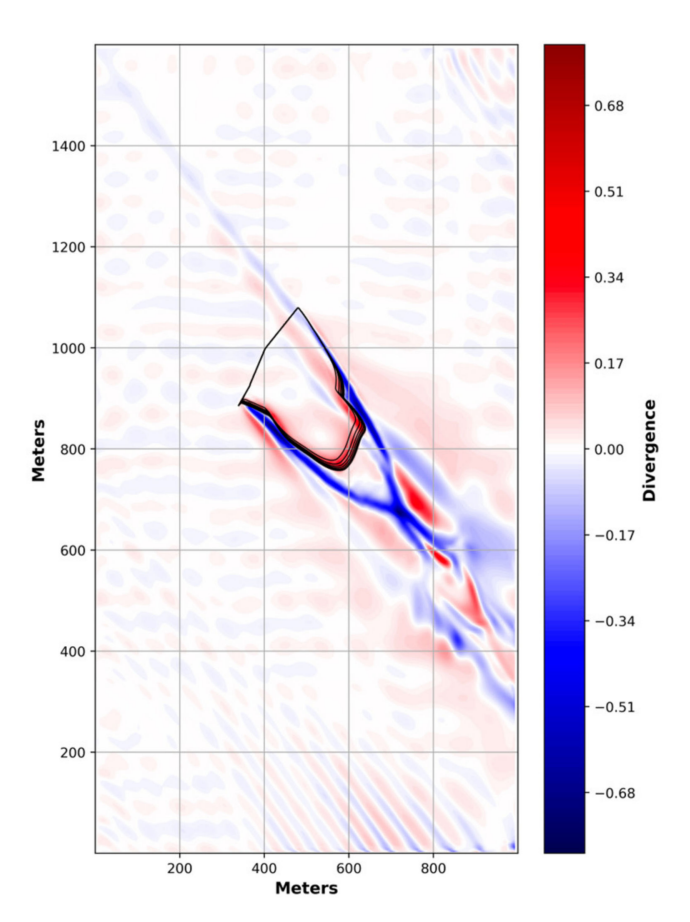


Figure 10. Surface divergence (red) and convergence (Blue) from the coupled FF2 simulation taken at 15:07:36 CST.

This effect is critical in controlling the shape of the fire and its ROS. It can be seen in Figure 11, which shows that the shape and the ROS of the fire are vastly different in the twoway coupled simulation (Figure 11a) than in the one-way coupled simulation (Figure 11b). This phenomenon is consistent with [14] and their one-way coupled and two-way coupled ROS comparisons. The lack of the convective column in the one-way coupled simulation (in which no heat is released into the atmosphere) results in more uniform and weaker local winds as well as slower fire propagation. Moreover, the difference in the fire-front shape indicates that the inflow into the pyro-convective column is responsible for the more parabolic fire shape, which is visible in the two-way coupled simulation. This was also seen in [11] where the shape of the fire front was affected by the fire-induced winds as the fire head become narrower and accelerated. Neglecting these winds reduces both the ROS and the curvature of the fire front, making it less realistic when compared to observations (see also Figure 4). The comparison between the one-way coupled simulation neglecting the fire impact on the wind field and the two-way coupled resolving the fire winds indicates that the horizontal circulation induced by the fire near its front significantly accelerates fire progression. For instance, at the time 15:08:00 the overall rate of spread of the coupled simulation was 1.50 m/s while in the uncoupled simulation it was only 1.04 m/s. Further examples of this phenomenon can be seen in Table 2 where the one-way coupled simulation consistently produced a slower ROS for all towers when compared to the two-way coupled simulation and the observations.

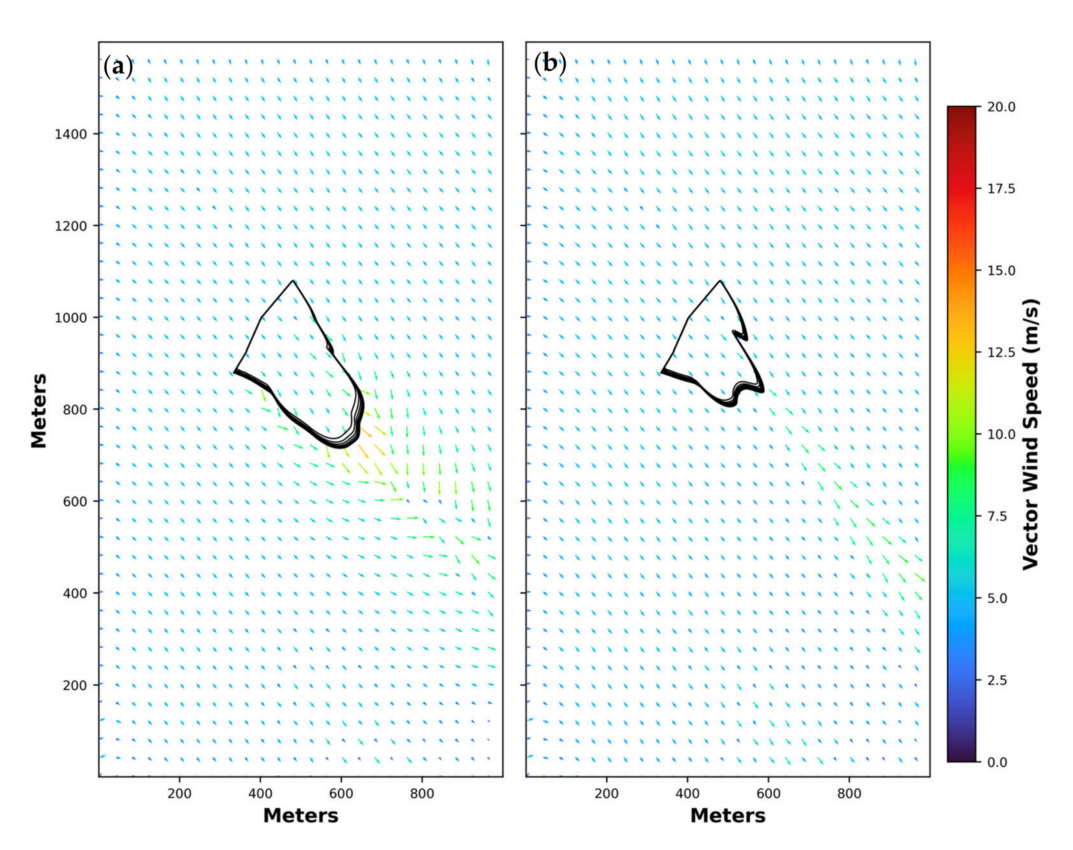


Figure 11. (a) Two-way coupled fire spread with color coded wind vectors according to the two-way coupled horizontal wind speed. (b) One-way coupled fire spread with color coded wind vectors according to the one-way coupled horizontal wind speed. The black contours represent the fire-front position. Both images were taken at 15:08:00 CST.

3.4.2. Analysis of the Thermal Plume Structure at the Flanks

After analyzing the temperature and circulations at the head fire, we focused on the flanks of the fire. The thermal structure of the atmosphere there has a different characteristic than the one over the fire head. The fire-induced temperature perturbations remained elevated for a longer period, and the fire heated the surrounding atmosphere for a longer period, as seen in Figure 12. In the simulation, the duration of the thermal perturbation did not last as long at the WT (about 70 s in the observations in Figure 12b, and 50 s in the simulation in Figure 12a). This was likely due to a larger burning zone (longer residence time) in the observations compared to the simulation. As for the vertical extent, there were no tall towers located at the flanks of the fire in this experiment, which limits the amount of data at higher heights. However, even based on the lower levels of the fire, it is evident that the model struggled to resolve the temperatures at the WT, which reached 220 °C up to 2 m above the ground in observations, but only $110\,^{\circ}$ C in the simulation. We hypothesize that the misalignment between the simulated and observed main axis of the fire propagation after the wind shift led to the discrepancies in the thermal perturbations between the observations and simulation at the WT.

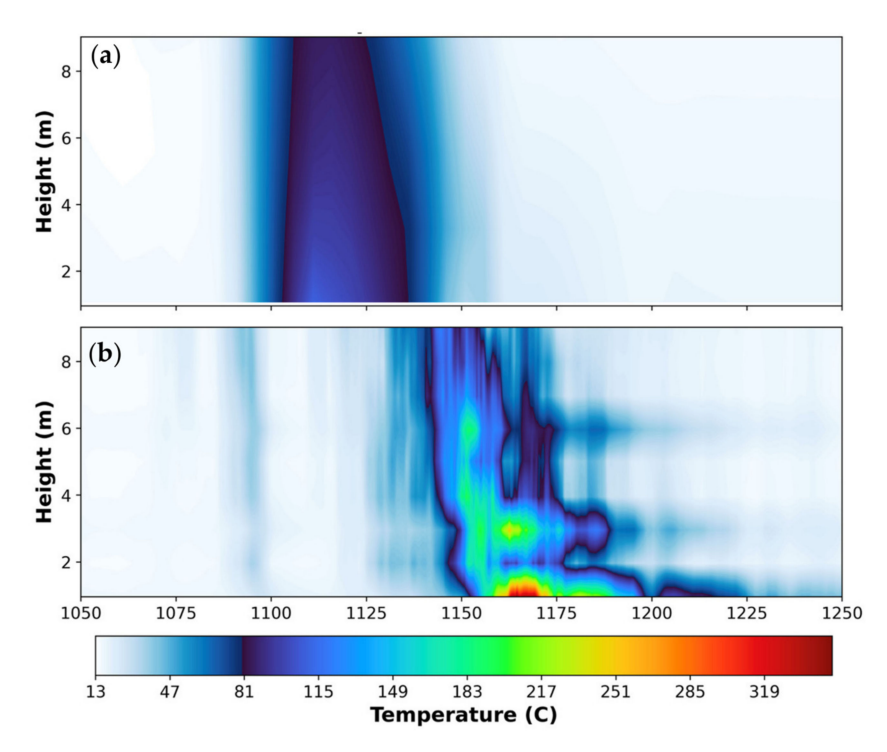


Figure 12. Time series of the temperature (a) from the simulation and (b) 10 s rolling average of the temperature from the observations at the WT.

3.4.3. Circulations at the Flanks of the Fire

To analyze the circulations at the flanks of the fire, two cross-sections were created that cut through the flanks of the fire (as seen in Figures 13a and 14a). These cross-sections consisted of temperature and wind in Figure 13b and wind and fire-induced vertical wind in Figure 14b. The cross-section shown in Figure 13b indicates two buoyant plumes located directly over the two flanks of the fire. The left (south-western) flank burned hotter than the right (north-eastern) flank (140 °C compared to 45 °C) and produced a more vigorous plume than the right flank. This asymmetry caused the weak flow along the cross-section plane as seen in Figure 13b in the right to left direction. This flow explains why the left (south-western) flank burned hotter than the right flank. This flow was pushing the left flank toward unburned fuel, while the right (north-eastern) flank was pushed away from the fuel into the area that had already been burned. This decreased the temperature and the updraft over the right flank, as seen in Figure 14b. Although the fire flanks produced significant vertical velocities reaching over 6 m/s, they did not produce as strong of a cross-fire flow as was observed near the fire head. As a result, flanks did not experience the impact of the fire-induced circulation like the fire head. As can be seen in Figure 11, the flanks were represented similarly in the two-way coupled and one-way coupled simulations because the main flow was in the direction roughly normal to the flanks, so there was no mechanism to push the convective columns away from the fire, and to allow the inflow into the base of convective column accelerate winds over the fire front. This can be seen in Figure 14b, which shows that the cores of the convective columns with strongest vertical velocities were located directly over the southern (left) flank, and there was no significant wind induced over the fire due to the alignment between the convergence zone and the location of the fire front.

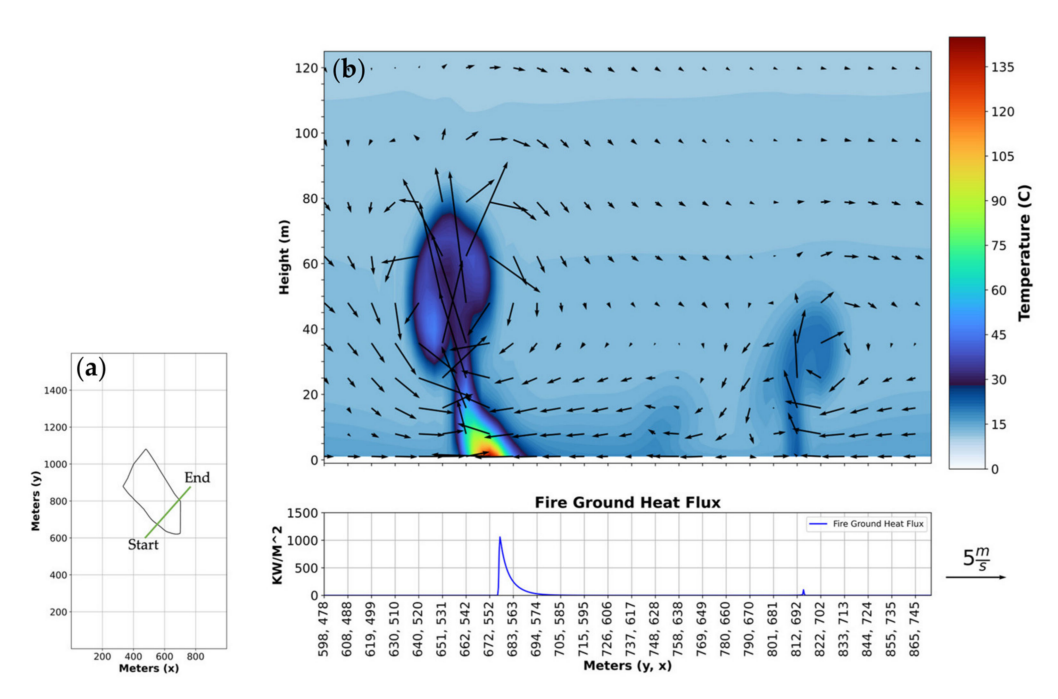


Figure 13. (a) Fire-front position (black polygon) and the orientation of the cross-section (green line). (b) Vertical cross-section showing the temperature and winds from the two-way coupled simulation at the flanks of the fire and the fire ground heat flux showing the position and intensity of the fire taken at 15:09:11 CST. The size of the arrows corresponds to the intensity in wind speed.

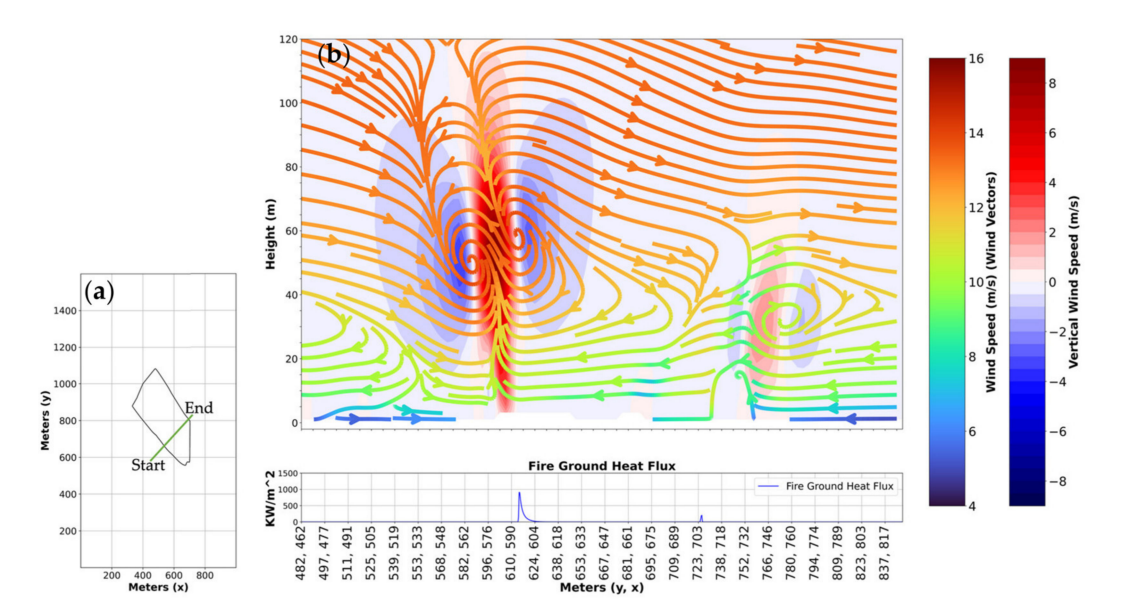


Figure 14. (a) Fire-front position (black polygon) and the orientation of the cross-section (green line). (b) Vertical cross-section showing winds and the fire ground heat flux showing the position and intensity of the fire from the two-way coupled simulation taken at 15:10:11 CST. The streamlines are color coded according to the wind speed magnitude; the shading shows the magnitude of the fire-induced vertical velocity.

The two updrafts occurring at both flanks created counterrotating vortices notable in Figures 13b and 14b, which were observed during the experiment. The most prominent vortices occurred over the left flank due to it burning significantly hotter than the right flank. The greater heat release generated the taller plume which created lower pressure near the surface due to the hot air moving up. Air then rushed in to fill the new void, which created these circulating flow patterns in Figures 13b and 14b. The right flank did

not generate as much heat as the left flanks, so the winds are much weaker at the right flank. A similar pattern was still seen there with a circulating flow; however, it is not as prominent at the right flank as it is at the left flank. It has to be noted that, in the flank circulation, the updrafts occurred over the fire front whereas, in the head circulation, the updrafts occurred ahead of the fire. As a result of the convergent flows occurring at the fire front instead of ahead of it, there was no evident impact of fire-induced winds on the flank propagation as opposed to the fire head (see Figure 10).

4. Conclusions

In this study, we used the FF2 observations as well as numerical simulations performed with WRF-SFIRE to investigate the fire-induced perturbations in winds and temperature at the fire head and at the flanks during moderate winds (10–12 m/s). To determine the fire-induced circulations, two idealized simulations were used. The two-way coupled one where the fire heat and moisture fluxes were fed into the atmosphere and the one-way coupled, in which atmospheric winds were used to drive the fire propagation, but fire fluxes were not injected into the atmosphere. The differences between these simulations allowed us to quantify the fire effects on the local meteorology near the head of the fire and near the flanks.

The comparison between the simulated and observed fire progression indicates that the model realistically captured the timing of the FFP through the MT and the initial ROS matched nearly perfectly with the observations (1.04 m/s compared to 1.00 m/s). The rate of fire head progression towards the ET was overestimated by about 8.6% (1.45 m/s compared to 1.33 m/s). However, later into the experiment, the timing of the flank passages through the west and south towers were simulated with smaller accuracy, most probably due to the wind direction shift that happened during the burn but could not be implemented in the idealized simulation. This resulted in differences in the shape of the fire between the simulation and observations later in the simulation, and errors in the simulated timing of the flank passage through the short towers.

However, our main focus was on the vertical structures of the plume at the MT and ET which were captured realistically in terms of the temperature range, as well as vertical and horizontal plume extent. Despite discrepancies between the simulated lateral fire extent and observations, the simulation accurately predicted the structure of the thermal plume with temperatures profiles similar to the observed temperatures at the head of the fire. The widths of the thermal plume were resolved realistically. These thermal plumes then generated updrafts which changed both the horizontal and vertical wind velocities near the fire front. However, the analysis of the vertical velocities indicates that during the FFP through the first tower (about 60 s from the ignition start) the flow was not fully resolved yet.

The numerical simulations were used to analyze the fire-induced circulations at the head and flanks of the fire, and to investigate their impact on fire propagation. At the fire head, the strongest fire winds occurred near the surface and decreased with height. As the fire heated up the surrounding atmosphere, it created hot air masses which were driven up due to buoyant forcing. Consequently, this forcing generated updrafts as strong as 6.1 m/s, which were pushed ahead of the fire front by the ambient wind. Strong surface convergence occurred ahead of the fire front and induced a cross-fire flow. This flow directly affected the ROS, as the accelerated winds over the fire increased the rate of spread. The horizontal fire-induced winds reached 3.3 m/s and increased the ambient winds by around 37.3%. The uncoupled simulations confirmed that without this effect, the fire would spread approximately 36.2% slower. This effect also led to the reversal of the typical logarithmic vertical wind profile during the FFP leading to the wind speed being the strongest at the surface and decreasing with height.

The inclusion of the two-way coupling, which allowed us to resolve fire winds, significantly improved the representation of fire behavior. The underestimation in the fire propagation speed in one-way coupled simulation reaching on average 43%, was reduced to just 6% in the two-way coupled run resolving the impact of fire winds on fire behavior.

The flanks of the fire did not spread as fast as the head fire since they did not generate as strong a cross-fire wind as the head, and the wind direction was approximately parallel to both flanks. As a result, the ROS values between two-way coupling and one-way coupling at the flanks were similar. The flanks of the fire experienced convergent flow at the fire front instead of ahead of the fire front like the head fire, which limited the cross-fire flow that could accelerate its progression.

It has to be noted that the presented results are based on the analysis of a relatively small grassfire. Although it is expected that the fire-induced circulations are similarly important during wildfires, the lack of comprehensive observations of micrometeorological conditions near the active wildfires precludes a rigorous analysis of fire-atmosphere interactions at much larger scales. However, as the data from larger experiments such as California Fire Dynamics Experiment (CalFiDe [22]) become available, a similar analysis of the impact of fire-atmosphere interactions on the wildfire dynamic will become possible.

Author Contributions: Conceptualization, A.K.K. and C.B.C.; methodology, A.K.K.; software, A.F. and J.T.B.; validation, J.T.B.; formal analysis, J.T.B., A.K.K. and J.D.M., investigation, J.T.B., A.K.K. and J.D.M.; resources, A.K.K. and C.B.C.; writing—original draft preparation, J.T.B.; writing—review and editing, J.T.B., A.K.K., C.B.C., J.D.M. and A.F.; visualization, J.T.B. and A.F.; supervision, A.K.K.; project administration, A.K.K.; funding acquisition, A.K.K. and C.B.C. All authors have read and agreed to the published version of the manuscript.

Funding: This research was performed under the auspices of the U.S. Department of Energy by Lawrence Livermore National Laboratory (LLNL) under Contract DE-AC52-07NA27344. This work was also supported in part by LLNL LDRD 20-ERD-034, NASA grants 80NSSC19K1091 and 80NSSC22K1717, NASA grant NNX12AD05A, CFDA No. 43.001 through BAER Institute, Wildfire Interdisciplinary Research Center grant 34-1505-0009 as well as CALFIRE grant 8GG21829.

Institutional Review Board Statement: Not applicable.

Informed Consent Statement: Not applicable.

Data Availability Statement: The WRF-SFIRE code used in the study is available from http://github.com/openwfm/WRF-SFIRE commit 3c960d725cfab7597bcfcdecb5bc55f70a7e640e. The FireFlux2 data are available per request from https://www.fireweather.org/data-request.

Acknowledgments: We would like to acknowledge high-performance computing support from Cheyenne (doi:10.5065/D6RX99HX) provided by NCAR's Computational and Information Systems Laboratory, sponsored by the National Science Foundation. We are also grateful to the SJSU Fire HPC Support group for providing the computational assistance needed to carry out the model analyses shown here.

Conflicts of Interest: The authors declare no conflict of interest.

References

- 1. Heilman, W.E.; Clements, C.B.; Seto, D.; Bian, X.; Clark, K.L.; Skowronski, N.S.; Hom, J.L. Observations of Fire-Induced Turbulence Regimes during Low-Intensity Wildland Fires in Forested Environments: Implications for Smoke Dispersion. *Atmos. Sci. Lett.* **2015**, *16*, 453–460. [CrossRef]
- 2. Kochanski, A.; Jenkins, M.A.; Sun, R.; Krueger, S.; Abedi, S.; Charney, J. The Importance of Low-Level Environmental Vertical Wind Shear to Wildfire Propagation: Proof of Concept. *J. Geophys. Res. Atmos.* **2013**, *118*, 8238–8252. [CrossRef]
- 3. Clements, C.; Seto, D. Observations of Fire–Atmosphere Interactions and Near-Surface Heat Transport on a Slope. *Boundary-Layer Meteorol.* **2014**, *154*, 409–426. [CrossRef]
- Clements, C.B.; Zhong, S.; Bian, X.; Heidman, W.E.; Byun, D.W. First Observations of Turbulence Generated by Grass Fires. J. Geophys. Res. Atmos. 2008, 113, D22102. [CrossRef]
- 5. Clements, C.B.; Kochanski, A.K.; Seto, D.; Davis, B.; Camacho, C.; Lareau, N.P.; Contezac, J.; Restaino, J.; Heilman, W.E.; Krueger, S.K.; et al. The FireFlux II Experiment: A Model-Guided Field Experiment to Improve Understanding of Fire-Atmosphere Interactions and Fire Spread. *Int. J. Wildland Fire* 2019, 28, 308–326. [CrossRef]
- 6. Costes, A.; Rodier, Q.; Masson, V.; Lac, C.; Rochoux, M.C. Effects of High-Density Gradients on Wildland Fire Behavior in Coupled Atmosphere-Fire Simulations. *Geosci. Model Dev.* **2022**, *14*, e2021MS002955. [CrossRef]
- 7. Tedim, F.; Leone, V.; Amraoui, M.; Bouillon, C.; Coughlan, M.R.; Delogu, G.M.; Fernandes, P.M.; Ferreira, C.; McCaffrey, S.; McGee, T.K.; et al. Defining Extreme Wildfire Events: Difficulties, Challenges, and Impacts. *Fire* **2018**, *1*, 9. [CrossRef]

8. Dupuy, J.-L.; Pimont, F.; Linn, R.; Clements, C. FIRETEC Evaluation against the FireFlux Experiment: Preliminary Results. In *Advances in Forest Fire Research*; ADAI: Coimbra, Portugal, 2014; pp. 261–274.

- 9. Kochanski, A.K.; Jenkins, M.A.; Mandel, J.; Beezley, J.D.; Clements, C.B.; Krueger, S. Evaluation of WRF-SFIRE Performance with Field Observations from the FireFlux Experiment. *Geosci. Model Dev.* **2013**, *6*, 1109–1126. [CrossRef]
- 10. Costes, A.; Rochoux, M.C.; Lac, C.; Masson, V. Subgrid-Scale Fire Front Reconstruction for Ensemble Coupled Atmosphere-Fire Simulations of the FireFlux I Experiment. *Fire Saf. J.* **2021**, 126, 103475. [CrossRef]
- 11. Filippi, J.-B.; Pialat, X.; Clements, C.B. Assessment of ForeFire/Meso-NH for Wildland Fire/Atmosphere Coupled Simulation of the FireFlux Experiment. *Proc. Combust. Inst.* **2013**, *34*, 2633–2640. [CrossRef]
- 12. Cheney, N.P.; Gould, J.S. Fire Growth in Grassland Fuels. Int. J. Wildland Fire 1995, 5, 237–247. [CrossRef]
- 13. Mell, W.; Jenkins, M.A.; Gould, J.; Cheney, P. A Physically Based Approach to Modeling Grassland Fires. *Int. J. Wildland Fire* **2006**, 16, 1–22. [CrossRef]
- 14. Sun, R.; Krueger, S.K.; Jenkins, M.A.; Zulauf, M.A.; Charney, J.J. The Importance of Fireatmosphere Coupling and Boundary-Layer Turbulence to Wildfire Spread. *Int. J. Wildland Fire* **2009**, *18*, 50–60. [CrossRef]
- 15. Clark, T.L.; Jenkins, M.A.; Coen, J.; Packham, D. A Coupled Atmosphere–Fire Model: Convective Feedback on Fire-Line Dynamics. *J. Appl. Meteorol.* **1996**, *35*, 875–901. [CrossRef]
- 16. Mandel, J.; Beezley, J.D.; Coen, J.L.; Kim, M. Data Assimilation for Wildland Fires. IEEE Control Syst. 2009, 29, 47-65.
- 17. Mandel, J.; Beezley, J.D.; Kochanski, A.K. Coupled Atmosphere-Wildland Fire Modeling with WRF 3.3 and SFIRE 2011. *Geosci. Model Dev.* **2011**, *4*, 591–610. [CrossRef]
- 18. Mandel, J.; Bennethum, L.S.; Beezley, J.D.; Coen, J.L.; Douglas, C.C.; Kim, M.; Vodacek, A. A Wildland Fire Model with Data Assimilation. *Math. Comput. Simul.* 2008, 79, 584–606. [CrossRef]
- 19. Rothermel, R.C. *A Mathematical Model for Predicting Fire Spread in Wildland Fuels*; Intermountain Forest and Range Experiment Station, Forest Service, United States Department of Agriculture: Ogden, UT, USA, 1972.
- 20. Kochanski, A.K.; Jenkins, M.A.; Mandel, J.; Beezley, J.D.; Krueger, S.K. Real Time Simulation of 2007 Santa Ana Fires. *For. Ecol. Manag.* **2013**, 294, 136–149. [CrossRef]
- 21. Mallia, D.V.; Kochanski, A.K.; Urbanski, S.P.; Mandel, J.; Farguell, A.; Krueger, S.K. Incorporating a Canopy Parameterization within a Coupled Fire-Atmosphere Model to Improve a Smoke Simulation for a Prescribed Burn. *Atmosphere* **2020**, *11*, 832. [CrossRef]
- 22. NOAA Chemical Sciences Laboratory. California Fire Dynamics Experiment (CalFiDE). Available online: https://csl.noaa.gov/groups/csl7/measurements/2022calfide/ (accessed on 9 August 2023).

Disclaimer/Publisher's Note: The statements, opinions and data contained in all publications are solely those of the individual author(s) and contributor(s) and not of MDPI and/or the editor(s). MDPI and/or the editor(s) disclaim responsibility for any injury to people or property resulting from any ideas, methods, instructions or products referred to in the content.